Biomimetic Nanocomposites

DOI: 10.1002/anie.201401072

Molecular Engineering of Fracture Energy Dissipating Sacrificial Bonds Into Cellulose Nanocrystal Nanocomposites**

Jason R. McKee, Johannes Huokuna, Lahja Martikainen, Mikko Karesoja, Antti Nykänen, Eero Kontturi, Heikki Tenhu, Janne Ruokolainen, and Olli Ikkala**

Abstract: *Even though nanocomposites have provided a plethora of routes to increase stiffness and strength, achieving increased toughness with suppressed catastrophic crack growth has remained more challenging. Inspired by the concepts of mechanically excellent natural nanomaterials, one-component nanocomposites were fabricated involving reinforcing colloidal nanorod cores with polymeric grafts containing supramolecular binding units. The concept is based on mechanically strong native cellulose nanocrystals (CNC) grafted with glassy polymethacrylate polymers, with side chains that contain 2-ureido-4[1H]-pyrimidone (UPy) pendant groups. The interdigitation of the grafts and the ensuing UPy hydrogen bonds bind the nanocomposite network together. Under stress, UPy groups act as sacrificial bonds: simultaneously providing adhesion between the CNCs while allowing them to first orient and then gradually slide past each other, thus dissipating fracture energy. We propose that this architecture involving supramolecular binding units within side chains of polymer grafts attached to colloidal reinforcements opens generic approaches for tough nanocomposites.*

In recent years, low-density natural nanocomposite materials such as silk, animal bone, and nacre have acted as an inspiration for material scientists, as they demonstrate remarkable toughness combined with stiffness and strength, which have been challenging to obtain with man-made low-density materials.[1–7] This is achieved through their self-assembled nanoscale structures where hard reinforcing domains are bound together by soft energy-dissipative domains involving hidden lengths and sacrificial bonds,[4] all balanced and working together in synergy. Various types of biomimetic materials have been described combining "hard" nanoscale sheet-like or fibrillar reinforcements with classic "soft" synthetic polymers.[8–14] This architecture typically leads to high modulus and strength values. In some cases, distinct yielding and high strain can also be observed in the stress-strain measurements.[12] However, direct studies to control the crack growth and pronounced toughening have been less addressed in biomimetic materials.[11,15–17] In this respect, novel molecular engineering approaches towards biomimetic toughness are needed to mimic sacrificial bonds and molecular architectures of biological matter to achieve suppression of catastrophic crack growth. Feasible tools are offered by advances in polymeric supramolecular chemistry,[18] as well as in tailored polymers[19] and soft matter.[20]

Nature has provided materials scientists with numerous hard nanoscale materials that can be used to mechanically reinforce biomimetic composites. Especially interesting are rod-like cellulose nanocrystals (CNC).[21–24] They demonstrate exceptional mechanical properties, with high modulus values, up to 140 GPa, and high tensile strengths, in addition to being widely available from sustainable resources. CNCs have high aspect ratios with lateral dimensions in the range of a few nanometres and lengths ranging from 50 nm to 300 nm. Recently, they have been blended within polymeric matrices yielding nanoreinforced composites leading to improved stiffness and strength.[9,10,24–28] With such materials, in order to attain the full benefit of stress transfer between the yielding phase and the hard reinforcing phase, as observed in nature, all components should be fully compatible. Any aggregation or flocculation of the hard phase can have an adverse effect on both the mechanical and optical properties. In this regard, chemical modification of the predominantly hydrophilic CNC surfaces enhances the stress-transfer process due to increased compatibility with synthetic polymers as well as allowing for the possibility of adding specific functionalities into the interface between the hard and soft domains.[25,28,29]

While the improved stiffness and strength have amply been demonstrated in CNC composites and, in more general, biomimetic composites, the mechanisms that allow fracture energy dissipation for promoted toughening are considerably less understood, as they involve subtle nanomechanics. The hidden lengths and sacrificial bonds in tough biological matter lead to suppression of catastrophic crack growth due to increased process zones near the crack tips, thus distributing the stress concentration to larger volumes.[30,31] This promoted toughening can manifest in stress-strain curves as a distinct maximum or even in a series of them, indicating sequences of

[*] J. R. McKee, J. Huokuna, L. Martikainen, Dr. A. Nykänen, Prof. J. Ruokolainen, Prof. O. Ikkala
Molecular Materials, Department of Applied Physics
Aalto University School of Science and Technology
(previously Helsinki University of Technology)
P.O. Box 15100, 00076 Aalto, Espoo (Finland)
E-mail: Janne.Ruokolainen@aalto.fi
Olli.Ikkala@aalto.fi
Homepage: http://physics.aalto.fi/groups/molmat/
J. Huokuna, M. Karesoja, Prof. H. Tenhu
Laboratory of Polymer Chemistry, Department of Chemistry
University of Helsinki, PB 55, 00014 HY Helsinki (Finland)
Dr. E. Kontturi
Department of Forest Products Technology, Aalto University
P. O. Box, 16300, 00076 Aalto, Espoo (Finland)

[**] Funding from Academy of Finland, ERC Adv. Grant, ERA-NET WoodWisdom, and the Finnish Funding Agency for Technology and Innovation.

Supporting information for this article is available on the WWW under http://dx.doi.org/10.1002/anie.201401072.

major plastic yieldings.[5] For example, animal bone is formed from hard mineralized collagen fibres bound together by a soft organic physically cross-linked protein matrix.[4,31] It demonstrates remarkable mechanical properties through a synergy between the energy-dissipative deformations in the yielding protein phase with ensuing stress-transfer to the hard phase. Ligaments and tendons are also formed from hierarchical structures based mainly on elastin and collagen fibres.[5] Ligaments and tendons demonstrate remarkable elastic properties with high ductility and the ability to transfer stress until the maximum stress. Silk is another nanocomposite material, formed from reinforcing nanocrystalline β-sheets bound to a soft protein matrix, consisting of less ordered nanodomains involving sacrificial hydrogen bonds and hidden lengths.[6,32,33] Therefore, to create a next generation CNC-based biomimetic nanocomposite, the material should, in addition to having nanosized reinforcing domains tightly connected to the soft phase, also contain sufficient amount of sacrificial bonds along the yielding polymer backbone to dissipate the fracture energy upon mechanical deformation. This should manifest as crack blunting and distinct yield maxima in stress strain curves, not yet shown in CNC-based supramolecular materials. Therefore new approaches and architectures are called for.

In accordance to the aforementioned biological architectures, our present concept was designed as follows: All polymer chains forming the soft "matrix" phase should be covalently connected to the hard phase, as suggested, for example, by silk where the soft yielding chains encompass the reinforcing β-sheets. This grafting also facilitates stress transfer to the hard phase. In other words, blends of CNCs and separate matrix polymers were explicitly excluded from the present concept. Consequently, we investigated a one-component system. The matrix polymer should also contain a set of physical interaction sites to form a system of sacrificial bonds. These sacrificial bonds were constructed according to supramolecular construction principles. They also provide mutual connectivity between the CNCs, thus increasing the mechanical strength and, most importantly, lead to fracture energy dissipation via the gradual cleavage of the sacrificial bonds upon progressing deformations (see later Figure 3 for a scheme). Therefore, we investigated rod-like CNCs grafted with long polymer brushes, which also formed the matrix polymer (Figure 1 a,b), as this one-component system would inevitably yield a homogeneous dispersion. The subsequent graft incorporated 2-ureido-4[1*H*]-pyrimidone pendant groups (UPy) (Figure 1 c) to act as sacrificial binding sites.[34] In more detail, a UPy-based methacrylate (UPyMA) was examined, as UPy has a high dimerization constant due to the four hydrogen bonding sites (greater than $10^{-6}\,\text{M}^{-1}$ in $CHCl_3$). UPy has been utilized for numerous advanced applications, including self-healing materials[28,35] and shape-memory polymers.[36] Supramolecular CNC-based materials have been recently shown by attaching UPy moieties to the CNC surfaces using small-molecular linkers.[28] By blending these UPy-modified CNCs with a soft rubbery telechelic poly(ethylene-*co*-butylene) matrix, which was functionalized with UPy endgroups, supramolecular UV-healable nanocomposite rubbers were fabricated. However, plastic toughening was not observed. Note that our architecture is conceptually different, as we do not have a separate matrix phase. Moreover, we suggest that the long polymer grafts form a favourable architecture of binding between the CNCs via interdigitation of the grafts and potentially allowing

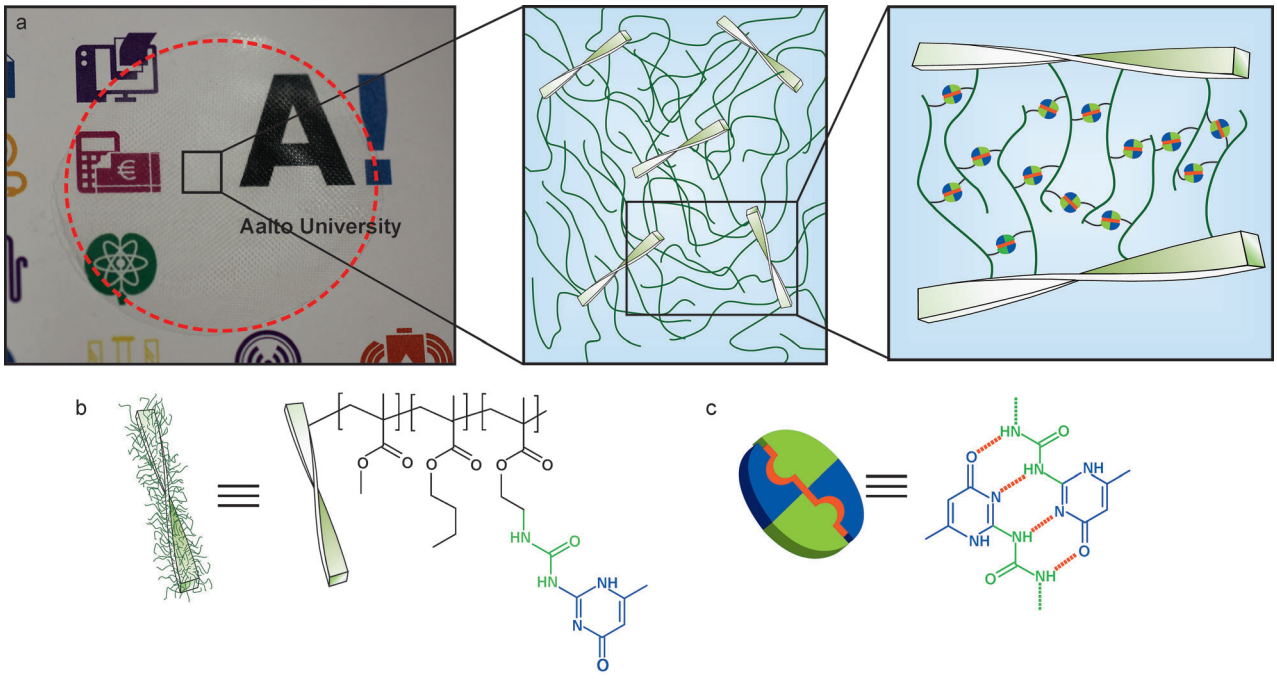

Figure 1. a) Transparency of a heat-pressed film of CNC-*g*-P(MMA-*r*-BMA-*r*-UPyMA). The film outer borders are visualized with red dashed line. b) Chemical composition of CNC-*g*-P(MMA-*r*-BMA-*r*-UPyMA). c) The dimerization of UPy by four hydrogen bonds.

"stick-slip" mutual sliding between the UPy-functionalized grafts (Figure 1a and Figure 3).

In more detail, a grafted architecture CNC-*g*-P(MMA-*r*-BMA-*r*-UPyMA) was formed containing random copolymer grafts consisting of methyl methacrylate (MMA), butyl methacrylate (BMA) and 2-ureido-4[1*H*]-pyrimidone methacrylate (UPyMA) monomers polymerized on CNCs by surface-initiated atom transfer radical polymerization (SI-ATRP) in DMF (see the Supporting Information for details). This work focuses solely on the brush composition MMA 69.0 mol.%, BMA 30.3 mol.%, and UPyMA 0.7 mol.%, as determined by ^{1}H NMR (Figure S1), as it allowed the most distinct yield phenomena (for other compositions, see Table S1). Feasibility of (meth)acrylic polymerization by SI-ATRP on CNCs is known from previous studies.[37,38] To remove the Cu^I-based catalytic component after the brush polymerization in DMF, the CNC-graft was precipitated in methanol at room temperature (21 °C) in order to leach out the copper residues (see the Supporting Information). The mean concentration of CNCs was estimated to be 2.5 ± 0.5 wt.% within the final composition based on the overall yield. According to dimethylformamide GPC, the weight-averaged molecular mass was 357 kg mol^{-1} (Figure S2). Also, due to the high insolubility of UPyMA at room temperature (21 °C), there were still some monomer impurities locked within the nanocomposite matrix that could not be fully extracted after purification. Based on these parameters, a mean grafting density of 0.2 ± 0.04 chains nm^{-2} was calculated, according to a method described earlier.[37] Further qualitative confirmation of the presence of UPy within the brushes was achieved by UV-Vis spectrometry. Here, a distinct signal was observed at 282 nm, corresponding to the previously published data on UPy[28]—signifying that the UPyMA had successfully been embedded within the methacrylic brush (Figure S3). In summary, we suggest that the structural units for the ensuing nanocomposite consisted of "hard" CNC cores bound together via "yielding" P(MMA-*r*-BMA-*r*-UPyMA) shells involving an assembly of "sacrificial" UPy pendant groups (Figure 1).

According to differential scanning calorimetry (DSC), the onset of glass transition (T_g) for CNC-*g*-P(MMA-*r*-BMA-*r*-UPyMA) was determined to be 63 °C (Figure S4). It should be noted that CNCs do not show any thermal transitions before degradation. Also, dynamic mechanical analysis (DMA) of CNC-*g*-P(MMA-*r*-BMA-*r*-UPyMA) indicated an onset of glass transition at roughly 63 °C with the storage modulus (E') dropping two orders of magnitude thereafter from 400 MPa at 60 °C to 2 MPa at 100 °C (Figure S5). Therefore, the side chain brush shell is in the glassy state at room temperature (21 °C).

According to DMA, $\tan\delta$ (E''/E') demonstrates a maximum near 95 °C (Figure S6). Indeed, at 100 °C the material turned soft enough to be heat-pressed into macroscopically homogeneous transparent films (Figure 1a). Curiously, a closer look at $\tan\delta$, in fact, suggests an overlapping bimodal thermal transition (Figure S6). This might be explained by two processes working together: first the thermal cleaving of the hydrogen bonds between UPy motifs, closely followed by the promoted thermal motion of the P(MMA-r-BMA-*r*-UPyMA) grafts.[36] These observations indirectly suggest that UPyMA had indeed been successfully embedded as a physical cross-linker into the yielding phase.

The present one-component nanocomposites behaved in a similar fashion to thermoplastic polymers by not being susceptible to phase separation. Tensile deformation of the heat pressed 100 μm thick films revealed pronounced plastic behavior in the shape of the stress-strain curves and directly showed how the cracks propagated. The stress-strain curves indicate an existence of major plastic deformation as a distinct yield peak at about 3% strain (Figure 2), unlike other supramolecular CNC materials, which have demonstrated only limited plastic deformation, typically in the form of a slope change in the stress-strain curve.[26,28] The maximum in the stress-strain curve at 29.0 ± 3.0 MPa indicates pronounced yielding, with a Young's modulus of 1.5 ± 0.2 GPa. The low

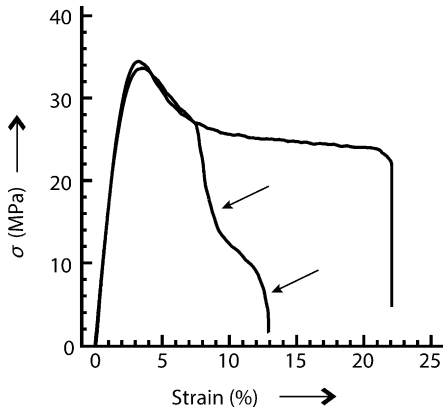

Figure 2. Examples of tensile stress-strain curves from parallel measurements for CNC-*g*-P(MMA-*r*-BMA-*r*-UPyMA) films, demonstrating occurrence of several sequential steps, see the arrows, also indicating sequences of dissipative noncatastrophic growths of the cracks.

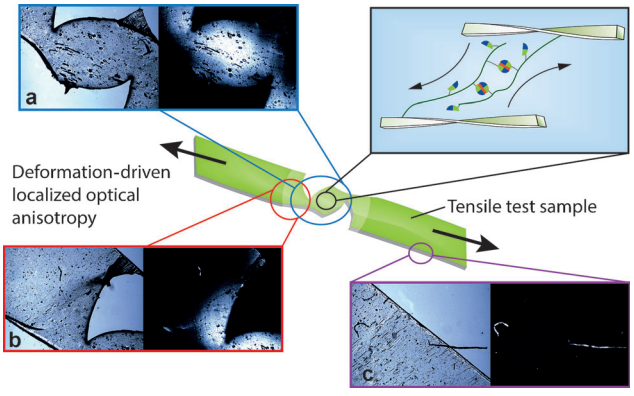

Figure 3. Examples of tortuous crack shapes and birefringence of CNC-*g*-P(MMA-*r*-BMA-*r*-UPyMA) test piece after tensile deformation. The left sides of panels (a–c) show optical micrographs from different positions of a sample undergoing a fracture process, and the scheme in the center shows their positions in the particular test specimen. a and b) Polarized optical micrographs demonstrate localized birefringence at sites of high deformation. c) However, the undeformed parts remained optically isotropic. Upper right, the suggested concept for two CNC-*g*-P(MMA-*r*-BMA-*r*-UPyMA)s sliding past each other with the complementary brushes slowly unzipping leading to mechanical cleaving of the UPy motifs (suggested stick–slip mechanism).

strength did not come as a surprise when taking into consideration the low weight fraction of the CNC in the final composition (2.5 ± 0.5 wt.%) as well as the supramolecular nature of the graft. The maximum strain was relatively large and demonstrated large variability from 8 to 24% between parallel samples; see Figure 2 for examples. Another indication of fracture energy dissipating plastic behavior was that in some samples, the fracture took place in sequences (see arrows in Figure 2), as seen in some biological materials.[5] Plastic deformations should also manifest as hysteretic behavior in cycled stress-strain curves. This hysteresis can be seen in cycled stress-strain deformations, even at small strains in the linear region before the main yield point (Figure S7). This is further evidence of the presence of dissipative processes upon deformation.

To illustrate the roles of the hydrogen bonding UPy groups had on the nanocomposite material's plastic deformation, a reference sample of CNC-P(MMA-*r*-BMA), without UPy, was prepared under the same synthetic conditions (Figure S8). Although the resulting reference sample without UPy physical cross-links had a relatively high tensile strength (10–38 MPa) and Young's modulus (2.7 ± 1.9 GPa), it was highly brittle (max strain: 0.4–1.6%) and did not demonstrate any plastic deformation.

Direct visualization of toughening was obtained by following the crack growth at the strain levels of 8–24% beyond the yield point. The cracks propagated slowly and not catastrophically (Figure 3), as accompanied by a strong stress whitening next to the cracks, as resolved visually and using polarized optical microscopy (POM) (Figure 3 and Figure S9). The stress whitening extended macroscopic distances (millimetres) beyond the crack tip, which signals extended process zones to distribute the stress concentration. This would indeed be expected with such toughened materials, and is also observed in hydrated nacre.[7] POM showed that the material was optically isotropic far from the crack tip, whereas the strongly deformed areas near the crack tip exhibited clear birefringence (Figure 3). We suggest that the UPy-based physical cross-links kept the yielding phase from fracturing, and allowed the CNCs to first mutually align and then gradually slide past each other, constantly working against the deformation by dissipating energy (Figure 3 upper right).

Finally, the cracks were investigated using electron microscopy. First, scanning electron microscopy (SEM) demonstrates rough crack surfaces, and near the crack tips evidence of aligned CNCs can be observed on the crack surface (Figure 4a, Figure S10). In addition, sets of extended voids are observed to open roughly in the parallel direction to the slowly progressing crack surface (Figure 4a). These voids are also expected to dissipate fracture energy. Furthermore, a closer look at the fracture surfaces demonstrate serrated surfaces, indicating pull-out mechanisms associated to nano-reinforced materials (Figure 4b,c).[12] Finally, TEM images of uniaxially elongated 500 nm thick films, as prepared by the fragility test methodology (see the Supporting Information for additional information), highlighted the crack mechanics. Figure 4c demonstrated the serrated crack surfaces, further emphasizing the reinforcing pull-out mechanisms of the colloidal CNCs (see arrows for pull-outs bridging the cracked surfaces). At the ends of the formed micron-sized cracks, numerous filaments of plastic deformation propagated parallel to the formed void to extend the process zones (Figure 4d). This observation indicates a distribution of fracture energy, meaning that the applied stress is partially diverted away from the fracture end.

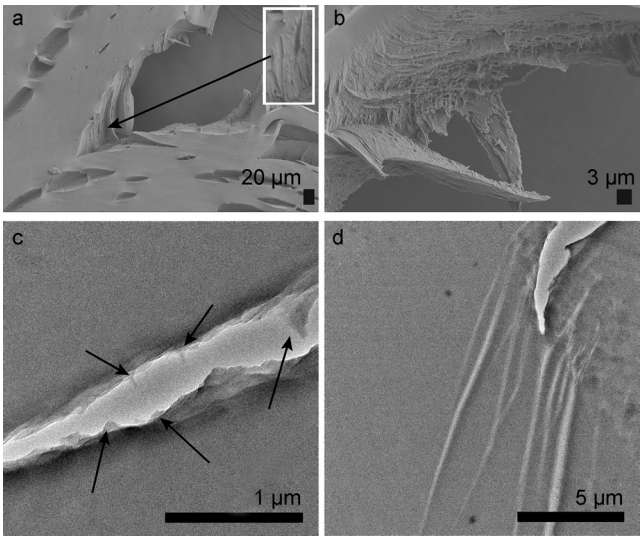

Figure 4. a) SEM image of fracture surface after uniaxial stress. Note that aligned fibrillar structures are observed near the crack tips, suggesting aligned CNCs. See Figure S10 for a larger image on the insert. b) Serrated surface features within the fracture surfaces indicating pull-out mechanisms based on SEM. c) TEM images of micron-sized cracks after uniaxial elongation of 500 nm thick slices of CNC-*g*-P(MMA-*r*-BMA-*r*-UPyMA) films, showing pull-outs (see arrows). d) Crack end demonstrating numerous filaments of plastic deformations spreading away from the crack end to extend the process zone (TEM micrograph).

In conclusion, we have demonstrated one-component biomimetic nanocomposites, consisting of reinforcing colloidal CNC cores and acrylate polymer shells, involving a set of hydrogen bonding UPy-moieties to form sacrificial bonds within the grafted brush architecture. This system demonstrated pronounced yields, non-catastropic growth of cracks, and dissipative deformation under tensile stress. We suggest that upon tensile deformation, the brush-modified CNCs first orient parallel to each other; and then the UPy motifs act as sacrificial bonds between the sliding CNCs, thus dissipating mechanical deformation energy. The grafted architecture, in general, also allows for large amounts of sacrificial bonds to be embedded into the system in addition to yielding a homogeneous dispersion of CNCs bound together by the interdigitation of the supramolecular grafts. We be believe that a one-component core–shell approach with polymer grafting approach involving a set of supramolecular sacrificial bonds is a feasible generic approach for the next-generation synthetic tough bio-nanomaterials.

Received: January 31, 2014
Published online: April 6, 2014

Keywords: biomimetic materials · cellulose nanocrystals · nanocomposite · supramolecular chemistry

[1] P. Fratzl, R. Weinkamer, *Prog. Mater. Sci.* **2007**, *52*, 1263 – 1334.
[2] B. Bhushan, *Philos. Trans. R. Soc. London Ser. A* **2009**, *367*, 1445 – 1486.
[3] H. D. Espinosa, J. E. Rim, F. Barthelat, M. J. Buehler, *Prog. Mater. Sci.* **2009**, *54*, 1059 – 1100.
[4] G. E. Fantner, T. Hassenkam, J. H. Kindt, J. C. Weaver, H. Birkedal, L. Pechenik, J. A. Cutroni, G. A. G. Cidade, G. D. Stucky, D. E. Morse, et al., *Nat. Mater.* **2005**, *4*, 612 – 616.
[5] M. A. Meyers, P.-Y. Chen, A. Y.-M. Lin, Y. Seki, *Prog. Mater. Sci.* **2008**, *53*, 1 – 206.
[6] S. Keten, Z. Xu, B. Ihle, M. J. Buehler, *Nat. Mater.* **2010**, *9*, 359 – 367.
[7] G. Mayer, *Science* **2005**, *310*, 1144 – 1147.
[8] Z. Tang, N. A. Kotov, S. Magonov, B. Ozturk, *Nat. Mater.* **2003**, *2*, 413 – 418.
[9] J. R. Capadona, O. van den Berg, L. A. Capadona, M. Schroeter, S. J. Rowan, D. J. Tyler, C. Weder, *Nat. Nanotechnol.* **2007**, *2*, 765 – 769.
[10] J. R. Capadona, K. Shanmuganathan, D. J. Tyler, S. J. Rowan, C. Weder, *Science* **2008**, *319*, 1370 – 1374.
[11] E. Munch, M. E. Launey, D. H. Alsem, E. Saiz, A. P. Tomsia, R. O. Ritchie, *Science* **2008**, *322*, 1516 – 1520.
[12] L. J. Bonderer, A. R. Studart, L. J. Gauckler, *Science* **2008**, *319*, 1069 – 1073.
[13] A. Walther, I. Bjurhager, J. M. Malho, J. Ruokolainen, L. Berglund, O. Ikkala, *Angew. Chem.* **2010**, *122*, 6593 – 6599; *Angew. Chem. Int. Ed.* **2010**, *49*, 6448 – 6453.
[14] R. M. Erb, R. Libanori, N. Rothfuchs, A. R. Studart, *Science* **2012**, *335*, 199 – 204.
[15] D. Sen, M. J. Buehler, *Sci. Rep.* **2011**, *1*, 35.
[16] J. M. Lackner, W. Waldhauser, B. Major, L. Major, M. Kot, *Thin Solid Films* **2013**, *534*, 417 – 425.
[17] M. J. Palmeri, K. W. Putz, L. C. Brinson, *ACS Nano* **2010**, *4*, 4256 – 4264.
[18] G. B. W. L. Ligthart, O. A. Scherman, R. P. Sijbesma, E. W. Meijer in *Macromolecular Engineering: Precise Synthesis Materials Properties, Applications, Vol. 1* (Eds.: K. Matyjaszewski, Y. Gnanou, L. Leibler), Wiley-VCH, Weinheim, **2007**, pp. 351 – 399.
[19] K. Matyjaszewski, J. Xia, *Chem. Rev.* **2001**, *101*, 2921 – 2990.
[20] A. M. Kushner, Z. Guan, *Angew. Chem.* **2011**, *123*, 9190 – 9223; *Angew. Chem. Int. Ed.* **2011**, *50*, 9026 – 9057.
[21] S. J. Eichhorn, *Soft Matter* **2011**, *7*, 303 – 315.
[22] Y. Habibi, L. A. Lucia, O. J. Rojas, *Chem. Rev.* **2010**, *110*, 3479 – 3500.
[23] K. Fleming, D. G. Gray, S. Matthews, *Chem. Eur. J.* **2001**, *7*, 1831 – 1835.
[24] N. Lin, J. Huang, A. Dufresne, *Nanoscale* **2012**, *4*, 3274 – 3294.
[25] H. Rosilo, E. Kontturi, J. Seitsonen, E. Kolehmainen, O. Ikkala, *Biomacromolecules* **2013**, *14*, 1547 – 1554.
[26] J. Fox, J. J. Wie, B. W. Greenland, S. Burattini, W. Hayes, H. M. Colquhoun, M. E. Mackay, S. J. Rowan, *J. Am. Chem. Soc.* **2012**, *134*, 5362 – 5368.
[27] K. Ben Azouz, E. C. Ramires, W. Van den Fonteyne, N. El Kissi, A. Dufresne, *ACS Macro Lett.* **2012**, *1*, 236 – 240.
[28] M. V. Biyani, E. J. Foster, C. Weder, *ACS Macro Lett.* **2013**, *2*, 236 – 240.
[29] S. Fujisawa, T. Saito, S. Kimura, T. Iwata, A. Isogai, *Biomacromolecules* **2013**, *14*, 1541 – 1546.
[30] M. E. Launey, R. O. Ritchie, *Adv. Mater.* **2009**, *21*, 2103 – 2110.
[31] M. E. Launey, M. J. Buehler, R. O. Ritchie, *Annu. Rev. Mater. Res.* **2010**, *40*, 25 – 53.
[32] J. D. van Beek, S. Hess, F. Vollrath, B. H. Meier, *Proc. Natl. Acad. Sci. USA* **2002**, *99*, 10266 – 10271.
[33] M. Heim, D. Keerl, T. Scheibel, *Angew. Chem.* **2009**, *121*, 3638 – 3650; *Angew. Chem. Int. Ed.* **2009**, *48*, 3584 – 3596.
[34] B. J. Folmer, R. P. Sijbesma, R. M. Versteegen, J. Van der Rijt, E. W. Meijer, *Adv. Mater.* **2000**, *12*, 874 – 878.
[35] J. Hentschel, A. M. Kushner, J. Ziller, Z. Guan, *Angew. Chem.* **2012**, *124*, 10713 – 10717; *Angew. Chem. Int. Ed.* **2012**, *51*, 10561 – 10565.
[36] T. Ware, K. Hearon, A. Lonnecker, K. L. Wooley, D. J. Maitland, W. Voit, *Macromolecules* **2012**, *45*, 1062 – 1069.
[37] J. Majoinen, A. Walther, J. R. McKee, E. Kontturi, V. Aseyev, J. M. Malho, J. Ruokolainen, O. Ikkala, *Biomacromolecules* **2011**, *12*, 2997 – 3006.
[38] J. R. McKee, E. A. Appel, J. Seitsonen, E. Kontturi, O. A. Scherman, O. Ikkala, *Adv. Funct. Mater.* **2014**, DOI: 10.1002/adfm.201303699.

